Compositional Embeddings for Multi-Label One-Shot Learning

Zeqian Li
Worcester Polytechnic Institute
zli14@wpi.edu

Michael Mozer
Google Brain
mcmozer@google.com

Jacob Whitehill
Worcester Polytechnic Institute
jrwhitehill@wpi.edu

Abstract

We present a compositional embedding framework that infers not just a single class per input image, but a set of classes, in the setting of one-shot learning. Specifically, we propose and evaluate several novel models consisting of (1) an embedding function f trained jointly with a "composition" function g that computes set union operations between the classes encoded in two embedding vectors; and (2) embedding f trained jointly with a "query" function h that computes whether the classes encoded in one embedding subsume the classes encoded in another embedding. In contrast to prior work, these models must both perceive the classes associated with the input examples and encode the relationships between different class label sets, and they are trained using only weak one-shot supervision consisting of the label-set relationships among training examples. Experiments on the OmniGlot, Open Images, and COCO datasets show that the proposed compositional embedding models outperform existing embedding methods. Our compositional embedding models have applications to multi-label object recognition for both one-shot and supervised learning.

1. Introduction

Embeddings, especially as enabled by advances in deep learning, have found widespread use in natural language processing, object recognition, face identification and verification, speaker verification and diarization, i.e., who is speaking when [28], and other areas. What embedding functions have in common is that they map their input into a fixed-length distributed representation (i.e., continuous space) that facilitates more efficient and accurate [27] downstream analysis than simplistic representations such as one-of-k (one-hot). Moreover, they are amenable to one-shot and few-shot learning since the set of classes that can be represented does not depend directly on the dimensionality of the embedding space.

The focus of most previous research on embeddings has been on cases where each example is associated with just one class (e.g., the image contains only one person's face).

In contrast, we investigate the case where each example is associated with not just one, but a *subset* of classes from a universe $\mathcal{S}$. Given 3 examples x_a, x_b and x_c, the goal is to embed each example so that questions of two types can be answered (see Fig. 1): (1) Is the set of classes in example x_a equal to the *union* of the classes in examples x_b and x_c? (2) Does the set of classes in example x_a *subsume* the set of classes in example x_b? For both these questions, we focus on settings in which the classes present in the example must be perceived automatically.

We approach this problem using *compositional embeddings*. Like traditional embeddings, we train a function f that maps each example $x \in \mathbb{R}^n$ into an embedding space $\mathbb{R}^m$ so that examples with the same classes are mapped close together and examples with different classes are mapped far apart. Unlike traditional embeddings, our function f is trained to represent the *set* of classes that is associated with each example, so that questions about set union and subsumption can be answered by comparing vectors in the embedding space. We do not assume that the mechanism by which examples are rendered from multiple classes is known. Rather, the rendering process must be learned from training data. We propose two models for one-shot learning, whereby f is trained jointly with either a "composition" function g that answers questions about set union, or a "query" function h that answers question about subsumption (see Figure 1). This work has applications to multi-object recognition in images: Given the embedding of an image x_a, answer whether x_a contains the object(s) in another image x_b, where the latter could contain classes that were never observed during training (i.e., one-shot learning). Storing just the embeddings but not the pixels could be more space-efficient and provide a form of image compression.

Contributions: To our best knowledge, our model is the first to perform multi-class one-shot learning using only weak supervision consisting of label-set relationships between training examples (in contrast to the strongly-supervised training approach in [1]; see the last section in Related Work). We explore how embedding functions can be trained both to *perceive* multiple objects that are possibly entangled (overlapping in space) and to *represent* them
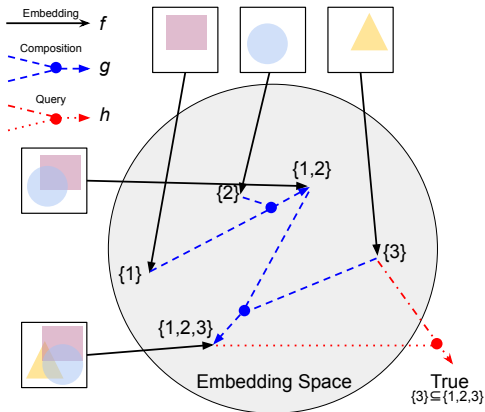
Figure 1: Overview: embedding function f is trained jointly with either a composition function g or a query function h. In particular, g's goal is to "compose" the embeddings of two examples, containing classes $\mathcal{T}$ and $\mathcal{U}$ respectively, to approximate the embedding of an example containing classes $\mathcal{T} \cup \mathcal{U}$.

so that set operations can be conducted among embedded vectors. We instantiate this idea in two ways – Model I for set union ($f\&g$) and Model II for set containment ($f\&h$) – and evaluate our models on visual domain. Our experiments show promising results that compositional embeddings can perceive and compute set relationships in highly challenging perceptual contexts. Since one-shot learning for multi-label classification is a new problem domain, we devise baseline methods based on traditional (non-compositional) embeddings, and our experiments provide evidence that compositional embeddings offer significant accuracy advantages. Finally, we explore applications of compositional embeddings to multi-label image classification for supervised (not one-shot) learning settings (Model III).

Supp. Material includes appendix and code is available in [1].

2. Related Work

Embeddings: We distinguish two types of embeddings: (1) "Perceptual" embeddings such as for vision (Facenet [26]) and speech (x-vector [29]), where each class (e.g., person whose voice was recorded or face was photographed) may contain widely varying examples across emotion, lighting, background noise, etc. (2) Item embeddings for words (word2vec [19], GloVe [22]), or for items & users in recommendation systems [5]; here, each class contains only one exemplar by definition. Within the former, the task of the embedding function is to map examples from the same

class close together and examples from other classes far apart. This often requires deep, non-linear transformations to be successful. With item embeddings, the class of each example does not need to be inferred; instead, the goal is to give the embedded vectors geometric structure to reflect co-occurrence, similarity in meaning, etc.

Compositional embeddings: Most prior work on compositionality in embedding models has focused on word embeddings [23, 21, 14, 10]. More recent work has explored "perceptual" embeddings: [6] combined embeddings from different sources in multimodal training. [12] proposed a model to infer the relative pose from embeddings of objects in the same scene. [32] proposed a method to decompose the attributes of one object into multiple representations. [2] introduced a method for generating judgments about compositional structure in embeddings. [31] showed that compositional information was deeply related to generalization in zero-shot learning. [30] proposed a way to train CNNs to learn features that had compositional property so that objects could be separated better from their surroundings and each other. [18] used compositional network embeddings to predict whether two new nodes in a graph, which were not observed during training, are adjacent, using node-based features as predictors.

Multi-label few-shot learning: The last few years have seen some emerging interest in the field of multi-label few-shot and zero-shot learning. [25] proposed a network to learn basic visual concepts and used compositional concepts to represent singleton objects not seen during training. Liu et al. [17] introduced an approach to infer compositional language descriptions of video activities and achieved zero-shot learning by composing seen descriptions. Huynh and Elhamifar [9] proposed a visual attention-based method for multi-label image classification that can generalize to classes not seen during training, but it requires auxiliary semantic vectors (e.g., attributes or word embeddings) associated with the unseen classes. The most similar work to ours is by Alfassy et al. [1]. Their model also tackles the problem of generating latent representations that reflect the set of labels associated with each input, and it also uses trained set operations (union, intersection, difference) that operate on pairs of examples. Algorithmically, our work differs from Alfassy's in several ways: Their method depends on strong supervision whereby the embedding and composition functions are trained using a fixed set of classes (they train on 64 classes from COCO), such that each image in the training set must be labeled w.r.t. *all* the classes in the *entire* training set. Their method also requires an extra multi-label classifier, and as a result they have 4 separate losses that are applied at different points during training. In contrast, our model requires only weak supervision: Each training episode has its own subset of classes, and each image in the episode must be labeled only w.r.t. that subset – there

is no need for it to be labeled w.r.t. all classes in the entire training set, or even for the set of training classes to be finite. Also, each of our models is trained using just 1 loss function. To emphasize, their approach requires class-labeled data for a fixed set of classes, whereas our approach requires merely sets of examples that possess certain compositional relationships.

3. Model I: Embedding f and Composition g

Assumptions and notation: For generality, we refer to the data to be embedded (images, videos, etc.) simply as "examples". Let the universe of classes be $\mathcal{S}$. From any subset $\mathcal{T} \subseteq \mathcal{S}$, a ground-truth rendering function $r : 2^{\mathcal{S}} \to \mathbb{R}^n$ "renders" an example, i.e., $r(\mathcal{T}) = x$. Inversely, there is also a ground-truth classification function $c : \mathbb{R}^n \to 2^{\mathcal{S}}$ that identifies the label set from the rendered example, i.e., $c(x) = \mathcal{T}$. Neither r nor c is observed. We let $e_{\mathcal{T}}$ represent the embedding (i.e., output of f) associated with some example containing classes $\mathcal{T}$.

Model: Given two examples x_a and x_b that are associated with singleton sets $\{s\}$ and $\{t\}$, respectively, the hope is that, for some third example x_c associated with *both* classes $\{s, t\}$, we have

$$g(f(x_a), f(x_b)) \approx f(x_c) \qquad (1)$$

Moreover, we hope that g can generalize to *any* number of classes within the set $\mathcal{S}$. For example, if example x_d is associated with a singleton set $\{u\}$ and x_e is an example associated with $\{s, t, u\}$, then we hope $g(g(f(x_a), f(x_b)), f(x_d)) \approx f(x_e)$.

There are two challenging tasks that f and g must solve cooperatively: (1) f has to learn to perceive multiple objects that appear simultaneously and are possibly non-linearly entangled with each other – all *without* knowing the rendering process r of how examples are formed or how classes are combined. (2) g has to define geometrical structure in the embedding space to support set unions. One way to understand our computational problem is the following: If f is invertible, then ideally we would want g to compute

$$g(e_{\mathcal{T}}, e_{\mathcal{U}}) = f(r(c(f^{-1}(e_{\mathcal{T}})) \cup c(f^{-1}(e_{\mathcal{U}})))). \qquad (2)$$

In other words, one way that g can perform well is to learn (without knowing r or c) to do the following: (1) invert each of the two input embeddings; (2) classify the two corresponding label sets; (3) render an example with the union of the two inferred label sets; and (4) embed the result. Training f and g jointly may also ensure systematicity of the embedding space such that any combination of objects can be embedded.

One-shot learning: Model I can be used for one-shot learning on a set of classes $\mathcal{N} \subset \mathcal{S}$ not seen during training in the following way: We obtain k labeled examples $x_1, \ldots, x_k$ from the user, where each $\{s_i\} = c(x_i)$ is the singleton set formed from the ith element of $\mathcal{N}$ and $|\mathcal{N}| = k$. We call these examples the *reference examples*. (Note that $\mathcal{N}$ typically changes during each episode; hence, these reference examples provide only a weak form of supervision about the class labels.) We then infer which set of classes is represented by a new example x' using the following procedure: (1) Compute the embedding of x', i.e., $f(x')$. (2) Use f to compute the embedding of each singleton example x_i, i.e., $e_{\{i\}} = f(x_i)$. (3) From $e_{\{1\}}, \ldots, e_{\{k\}}$, estimate the embedding of *every* subset $\mathcal{T} = \{s_1, \ldots, s_l\} \subseteq \mathcal{N}$ according to the recurrence relation:

$$e_{\{s_1, \ldots, s_l\}} = g(e_{\{s_1, \ldots, s_{l-1}\}}, e_{\{s_l\}}) \qquad (3)$$

Finally, (4) estimate the label of x' as

$$\underset{\mathcal{T} \subseteq \mathcal{N}}{\arg\min} |f(x') - e_{\mathcal{T}}|_2^2 \qquad (4)$$

3.1. Training Procedure

Functions f and g are trained jointly: For each example x associated with classes $\mathcal{T}$, we compute $e_{\mathcal{T}}$ from the singleton reference examples according to Eq. 3. (To decide the order in which we apply the recursion, we define an arbitrary ordering over the elements of $\mathcal{N}$ and iterate accordingly.) We then compute a triplet loss

$$\max(0, ||f(x) - e_{\mathcal{T}}||_2 - ||f(x) - e_{\mathcal{T}'}||_2 + \epsilon) \qquad (5)$$

for every $\mathcal{T}' \neq \mathcal{T} \subseteq \mathcal{N}$, where ϵ is a small positive real number [33, 26]. In practice, for each example x, we randomly pick some $\mathcal{T}' \in 2^{\mathcal{N}}$ for comparison. Both f and g are optimized jointly in backpropagation because the loss function is applied to embeddings generated from both.

Note that we also tried another method of training f and g with the explicit goal of encouraging g to map $e_{\mathcal{T}}$ and $e_{\mathcal{U}}$ to be close to $e_{\mathcal{T} \cup \mathcal{U}}$. This can be done by training f and g alternately, or by training them jointly in the same backpropagation. However, this approach yielded very poor results. A possible explanation is that g could fulfill its goal by mapping all vectors to the same location (e.g., $\mathbf{0}$). Hence, with this training method, a trade-off arose between g's goal and f's goal (separating examples with distinct label sets).

3.2. Experiment 1: OmniGlot

We first evaluated our method on the OmniGlot dataset [15]. OmniGlot contains handwritten characters from 50 different alphabets; in total it comprises 1623 symbols, each of which was drawn by 20 people and rendered as a 64×64 image. OmniGlot has been widely used in one-shot learning research (e.g., [24, 3]).

In our experiment, the model is provided with one reference image for each singleton test class (5 classes in total). Then, f and g are used to select the subset of classes that most closely match the embedding of each test example

(Eq. 4). The goal is to train f and g so that, on classes not seen during training, the exact set of classes contained in each test example can be inferred.

We assessed to what extent the proposed model can capture set union operations. To create each example with label set $\mathcal{T}$, the rendering function r randomly picks one of the 20 exemplars from each class $s \in \mathcal{T}$ and then randomly shifts, scales, and rotates it. Then, r computes the pixel-wise minimum across all the constituent images (one for each element of $\mathcal{T}$). Finally, r adds Gaussian noise. See Fig. 2 and Supp. Material. Due to the complexity of each character and the overlapping pen strokes in composite images, recognizing the class label sets is challenging even for humans, especially for $|\mathcal{T}| = 3$.

In this experiment, we let the total number of possible symbols in each episode be $k = 5$. We trained $f\&g$ such that the maximum class label set size was 3 (i.e., $|\mathcal{T}| \leq 3$). There are 25 such (non-empty) sets in total (5 singletons, $\binom{5}{2} = 10$ 2-sets, and $\binom{5}{3} = 10$ 3-sets).

Architecture: For f, we used ResNet-18 [7] that was modified to have 1 input channel and a 32-dimensional output. For g, we tested several architectures. First, define $\mathrm{Symm}(a, b; k) = W_1 a + W_1 b + W_2(a \odot b)$ to be a symmetric function[2] (with parameter matrices W_1, W_2) of its two examples $a, b \in \mathbb{R}^n$ that produces a vector in $\mathbb{R}^k$. We then defined four possible architectures for g:

- **Mean** (g_{Mean}): $\frac{(a+b)}{2} \rightarrow$ L2Norm.

- **Bi-linear** (g_{Lin}): $\mathrm{Symm}(a, b; 32) \rightarrow$ L2Norm.

- **Bi-linear + FC** ($g_{\mathrm{Lin+FC}}$): $\mathrm{Symm}(a, b; 32) \rightarrow \mathrm{BN} \rightarrow \mathrm{ReLU} \rightarrow \mathrm{FC}(32) \rightarrow$ L2Norm.

- **DNN** (g_{DNN}): $\mathrm{Symm}(a, b; 32) \rightarrow \mathrm{BN} \rightarrow \mathrm{ReLU} \rightarrow \mathrm{FC}(32) \rightarrow \mathrm{BN} \rightarrow \mathrm{ReLU} \rightarrow \mathrm{FC}(32) \rightarrow \mathrm{BN} \rightarrow \mathrm{ReLU} \rightarrow \mathrm{FC}(32) \rightarrow$ L2Norm.

BN is batch normalization, and $\mathrm{FC}(n)$ is a fully-connected layer with n neurons. We note that g_{Mean} is similar to the implicit compositionality found in word embedding models [19].

Training: For each mini-batch, $\mathcal{N}$ was created by randomly choosing 5 classes from the universe $\mathcal{S}$ (where $|\mathcal{S}| = 944$ in training set). Images from these classes are rendered using function r from either singleton, 2-set class label sets, or 3-set class label sets. In other words, $1 \leq |\mathcal{T}| \leq 3$ for all examples. See Supp. Material for details.

Testing: Testing data are generated similar to training data, but none of the classes were seen during training. We optimize Eq. 4 to estimate the label set for each test example.

---

[2]To be completely order-agnostic, g would have to be both symmetric and associative. Symmetry alone does not ensure $g(g(x, y), z) = g(x, g(y, z))$, but it provides at least some (if imperfect) invariance to order.

Baselines: Because multi-label few-shot learning is a new learning domain, and because none of the existing literature exactly matches the assumptions of our model ([1] assumes strongly supervised training labels, and [9] requires auxiliary semantic labels for unseen classes), it was not obvious to what baselines we should compare. When evaluating our models, we sought to assess the unique contribution of the *compositional* embedding above and beyond what traditional embedding methods achieve. We compared to two baselines:

1. **Traditional embedding f and average (TradEm)**: A reasonable hypothesis is that a traditional embedding function for one-shot learning trained on images with singleton class label sets can implicitly generalize to larger label sets by interpolating among the embedded vectors. Hence, we trained a traditional (i.e., non-compositional) embedding f just on singletons using one-shot learning, similar to [34, 11]. (Accuracy on singletons after training on OmniGlot: 97.9% top-1 accuracy in classifying test examples over 5 classes.) The embedding of a composite image with label set $\mathcal{T}$ is then estimated using the mean of the embeddings of each class in $\mathcal{T}$. In contrast to g_{Mean} above, the f in this baseline is trained by itself, without knowledge of how its embeddings will be composed.

   Note: In our experiments, the models always needed to pick the correct answer from 25 candidates. "1-sets" in the table means the accuracy when the ground truth is a singleton, but the model still sees 25 candidates.

2. **Most frequent (MF)**: Always guess the most frequent element in the test set. Since all classes occurred equally frequently, this was equivalent to random guessing. While simplistic, this baseline is useful to get a basic sense of how difficult the task is.

Assessment: We assessed accuracy (%-correct) in 3 ways: (a) Accuracy, over all test examples, of identifying $\mathcal{T}$. (b) Accuracy, over test examples for which $|\mathcal{T}| = l$ (where $l \in \{1, 2, 3\}$), of identifying $\mathcal{T}$. **Note**: we did *not* give the models the benefit of knowing $|\mathcal{T}|$ – each model predicted the class label set over *all* $\mathcal{T} \subset \mathcal{N}$ such that $|\mathcal{T}| \leq 3$. This can reveal whether a model is more accurate on examples with fewer vs. more classes. (c) Accuracy, over all examples, in determining just the *number* of classes in the set, i.e., $|\mathcal{T}|$.

Results: As shown in Table 1, the MF baseline accuracy was just 4% for an exact (top-1) and 12% for top-3 match. (Recall that the models did not "know" $|\mathcal{T}|$ and needed to pick the correct answer from all 25 possible label sets.) Using the TradEm approach, accuracy increased to 25.5% and 40.9%, respectively. All of the proposed $f\&g$ models strongly outperformed the TradEm baseline, indicating that training f jointly with a composition function is helpful. For all the $f\&g$ approaches as well as the TradEm baseline, model predictions were well above chance (MF) for all label

{1} {2} {3} {4} {5}

{1,2} {1,3} {1,4} {1,5} {2,3}

{2,4} {2,5} {3,4} {3,5} {4,5}

{1,2,3} {1,2,4} {1,2,5} {1,3,4} {1,3,5}

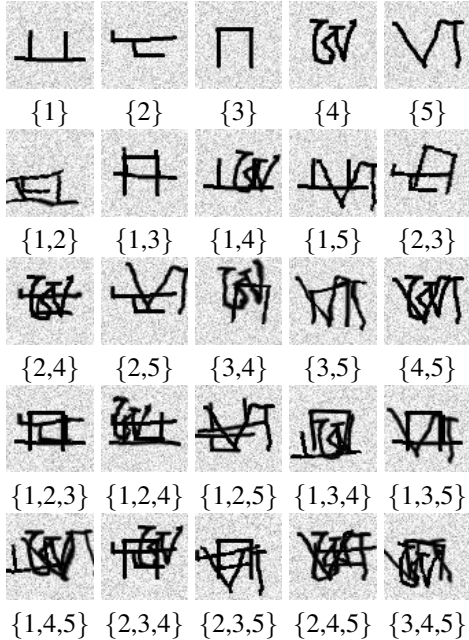{1,4,5} {2,3,4} {2,3,5} {2,4,5} {3,4,5}

Figure 2: Examples of the images from the OmniGlot dataset, used in Experiments 1 and 2. Below each image is its associated class label set $\mathcal{T}$.

set sizes, i.e., these approaches could all distinguish label sets with more than one element at least to some degree.

In terms of architecture for composition function g, overall, the g_{Lin}, which contains a symmetric bi-linear layer before L_2-normalization, did best: 64.7% and 87.6% for top-1 and top-3 matches over all examples, respectively. This suggests that composition by averaging alone is not optimal for this task. However, adding more layers (i.e., $g_{\text{Lin+FC}}$, g_{DNN}) did not help, especially when $|\mathcal{T}|$ increases. It is possible that the more complex g overfit, and that with regularization or more training data the deeper models might prevail.

Discussion: Experiments 1 suggests that, for $f\&g$ compositionality for set union, a simple linear layer works best. Function g_{Lin}, despite the L2Norm at the end, might retain a greater degree of associativity (i.e., $(a+b)+c = a+(b+c)$) than deeper g functions. This property may be important especially for larger $\mathcal{T}$, where g is invoked multiple times to create larger and larger set unions.

Scalability: The number of subsets is exponential in $|\mathcal{N}|$, which poses a scalability problem for both training and testing, and hence Model I may in some sense be regarded more as a proof-of-concept than practical algorithm. However, in settings where the number of simultaneously present classes is inherently small (e.g., in speaker diarization from audio signals, it is rare for more than just a few people to speak at once), the model can still be practical. In our Model II (Section 4), we overcome this scalability issue by switching

Experiment 1 (OmniGlot): Train with $|\mathcal{T}| \leq 3$

		Label Set Identification					
		$f\&g$ Approaches				Baselines	
		g_{DNN}	$g_{\text{Lin+FC}}$	g_{Lin}	g_{Mean}	TradEm	MF
All	Exact	50.6	56.7	**64.7**	52.8	25.5	4.0
	Top-3	76.5	81.7	**87.6**	80.0	40.9	12.0
1-sets	Exact	94.5	96.0	**97.0**	86.9	89.3	4.0
	Top-3	99.1	99.4	**99.6**	95.4	96.6	12.0
2-sets	Exact	51.2	54.6	**64.5**	49.7	15.4	4.0
	Top-3	82.9	83.0	**87.9**	81.4	37.7	12.0
3-sets	Exact	27.9	39.1	**48.9**	39.0	3.7	4.0
	Top-3	58.7	71.6	**81.1**	71.1	16.4	12.0
		Set Size Determination					
All		81.7	87.4	**90.1**	71.4	44.9	36.0

Table 1: Experiment 1 (OmniGlot): One-shot mean accuracy (% correct) of Model I in inferring the label set of each example exactly (top 1), within the top 3, and the size of each label set. Set Size Determination measures the ability to infer the set size. TradEm is similar to [34, 11], and MF is based on random guessing.

from set union to set containment.

4. Model II: Embedding f and Query h

With this model we explore compositional embeddings that implements *set containment*: In some applications, it may be more useful to determine whether an example *contains* an object or set of objects. For instance, we might want to know whether a specific object is contained in an image. Moreover, in some settings, it may be difficult during training to label every example (image, video, etc.) for the presence of *all* the objects it contains – for each example, we might only know its labels for a subset of classes. Here we propose a second type of compositional embedding mechanism that tests whether the set of classes associated with one example *subsumes* the set of classes associated with another example. We implement this using a "query" function h that takes two embedded examples as inputs: $h(f(x_a), f(x_b)) = \text{True} \iff c(x_b) \subseteq c(x_a)$. Note that h can be trained with only weak supervision w.r.t. the individual examples: it only needs to know *pairwise* information about which examples "subsume" other examples. Compared with typical multiple instance learning models, Model II deals with single samples instead of bags of instances. Additionally, training procedure of Model II is more focused on one-shot learning.

4.1. Training procedure

Functions f and h are trained jointly. Since h is not symmetric, its first layer is replaced with a linear layer

Experiment 2 (OmniGlot)

	h_{DNN}	$h_{\text{Lin+FC}}$	h_{Lin}	TradEm
Acc %	**71.8**	71.1	50.8	63.8
AUC	**80.0**	79.1	51.4	78.2

Table 2: One-shot learning results for Model II (with different versions of h) on OmniGlot compared to a traditional (non-compositional) embedding baseline (TradEm).

$W_1 a + W_2 b$ (see Supp. Material). In contrast to Model I, reference examples are not needed; only the subset relationships between label sets of pairs of examples are required. We backpropagate a binary cross-entropy loss, based on correctly answering the query defined above, through h to f.

4.2. Experiment 2: OmniGlot

Here we assess Model II on OmniGlot where size of class label sets is up to 5, and we use the same rendering function r in Experiment 1. Let $f(x_a)$ and $f(x_b)$ be the two arguments to h. For x_a, each image can be associated with multiple classes, from 1 class (i.e., $c(x_a) = \{s_1\}$) to 5 classes (i.e., $c(x_a) = \{s_1, s_2, \ldots, s_5\}$), where all label sets occur with equal frequency. For x_b (which is always a singleton in this experiment), half are positive examples (i.e., such that $h(f(x_a), f(x_b)) = \text{True}$) which are associated with classes contained in x_a, so that $c(x_b) \subseteq c(x_a)$. The other half are negative examples ($h(f(x_a), f(x_b)) = \text{False}$), where x_b is associated with some other singleton class $c(x_b) \not\subseteq c(x_a)$. Both the training set and test set have this configuration.

Architecture: The f was the same as in Experiment 1. For h, we tried several functions ($h_{\text{DNN}}, h_{\text{Lin+FC}}, h_{\text{Lin}}$), analogous to the different g from Section 3.2 except the final layers are 1-dim sigmoids. See Supp. Materials.

Baseline: How would we tackle this problem without compositional embeddings? We compared our method with a traditional (non-compositional) embedding method (**TradEm**) that is trained to separate examples according to their association with just a *single* class. In particular, for each composite example x_a (i.e., $|c(x_a)| = 2$), we picked one of the two classes arbitrarily (according to some fixed ordering on the elements of $\mathcal{S}$); call this class s_1. Then, we chose a positive example x_b (such that $c(x_b) = \{s_1\}$) and a negative example x_c (such that $c(x_c) = \{s_3\} \not\subseteq c(x_a)$). We then compute a triplet loss so the distance between $f(x_a)$ and $f(x_b)$ is smaller than the distance between $f(x_a)$ and $f(x_c)$, and backpropagate the loss through f. During testing, we use f to answer a query—does $c(x_a)$ contain $c(x_b)$?—by thresholding (0.5) the distance between $f(x_a)$ and $f(x_b)$.

Results are shown in Table 2. Compositional embeddings, as implemented with a combination of f trained jointly with either h_{DNN} or $h_{\text{Lin+FC}}$, outperform the TradEm baseline, in terms of both % correct accuracy and AUC.
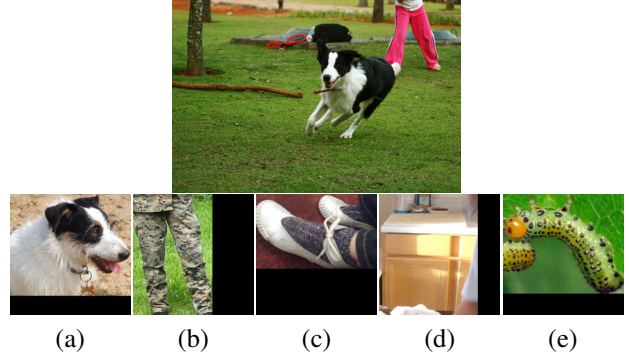

(a)   (b)   (c)   (d)   (e)

Figure 3: An example image (top) of a running dog and the lower body of a human. The image is padded to form a square and downscaled. The composite embedding with f is computed and then queried with h about the presence of the object in images (a-e), containing *dog*, *trousers*, *footwear*, *countertop*, and *caterpillar*. The query function h, when given the embeddings of the top image and another image, should return True for (a,b,c) and False for (d,e).

Unlike in Model I, where h_{Lin} achieved the best results, f trained jointly with h_{Lin} is just slightly better than random guess (50%). The deeper h worked better.

4.3. Experiment 3: Open Images

Here we trained and evaluated Model II on Open Images [13]. This dataset contains a total of 16M bounding boxes for 600 object classes on 1.9M images. This is a highly challenging problem: in the example in Fig. 3, f has to encode a dog, trousers and footwear; then, given completely different images of these classes (and others), h has to decide which objects were present in the original image. In Open Images, each image may contain objects from multiple classes, and each object has a bounding box. We acquire singleton samples by using the bounding boxes to crop singleton objects from images. In this experiment, 500 classes are selected for training and 73 other classes for testing. The training and evaluation settings are the same as Experiment 2.

Architectures: For f, we use ResNet-18 that was modified to have a 32-dimensional output. We used the same h as in Experiment 2.

Baselines:

1. **TradEmb**: Similar to Model II, here we compare with a non-compositional embedding trained using one-shot learning on singleton classes (**TradEm**). All objects are cropped according to their labeled bounding boxes and then resized and padded to 256×256. All original images are also resized and padded to the same size.

2. **SlideWin**: In Open Images, multiple objects co-occur in the same image but rarely overlap. Hence, one might

Experiment 3 (Open Images)

	h_{DNN}	$h_{\text{Lin+FC}}$	h_{Lin}	TradEm	SlideWin
Acc %	**76.9**	76.8	50.0	50.1	52.6
AUC	**85.4**	85.2	50.3	59.2	52.1

Table 3: One-shot learning results for Model II on Open Images compared to either the TradEm or the SlideWin baselines (similar to [8]).

wonder how well the following approach would work (somewhat similar to [8] on one-shot *detection*): train a traditional embedding model on examples of cropped objects; then apply it repeatedly to many "windows" within each test image (like a sliding window). To answer a query about whether the test image contains a certain object, compute the minimum (or median, or other statistic) distance between the embedding of each window and the embedding of the queried object.

We trained a baseline model using this approach (accuracy in 2-way forced-choice task on pre-cropped 256x256 images not seen during training: 93.6%). To answer queries, we partitioned each test image into a rectangular grid of at most 4x4 cells (depending on image aspect ratio). We then constructed windows corresponding to all possible contiguous subgrids (there were between 70-100 windows for each image), and then resized each window to 256x256 pixels. We found that taking the minimum embedding distance worked best.

Results are shown in Table 3. The compositional models of f combined with either h_{DNN} and $h_{\text{Lin+FC}}$ (though not with h_{Lin}) achieve an AUC of over 85% and easily outperform TradEm. It also outperforms the SlideWin method: even though this baseline was trained to be highly accurate on *pre-cropped* windows (as reported above), it was at-chance when forced to aggregate across many windows and answer the containment queries. It is also much more slower than the compositional embedding approach.

Discussion: An interesting phenomenon we discovered is that while the linear model g_{Lin} achieves the best results in the $f\&g$ setting (set union), it is hardly better than random chance for the $f\&h$ setting (set containment). On the other hand, while g_{DNN} is worse than other trainable g functions for set union, it outperforms the other functions for set containment. One possible explanation is that training f in Model I to distinguish explicitly between all possible subsets causes f to become very powerful (relative to the f in Model II), after which only a simple g is needed for set unions. The training procedure in Model II based on set containment might provide less information to f, thus requiring g to be more powerful to compensate. Another possibility
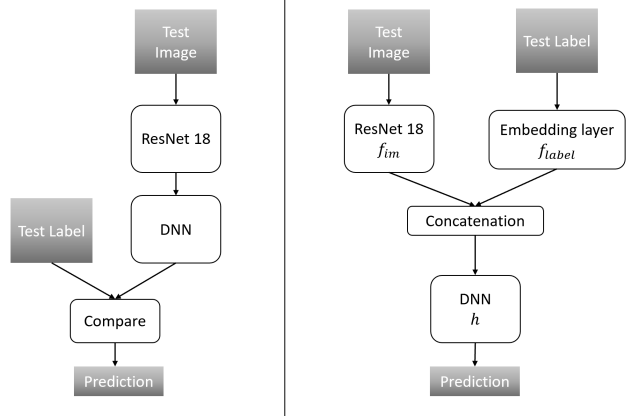

Figure 4: **Supervised multi-label image classification**: Left is a traditional approach based on a CNN with multiple independent sigmoid outputs. Right is the proposed Model III with 3 jointly trained embeddings f_{im}, f_{label}, & h.

is that, since g is applied recursively to construct unions, its complexity must be kept small to avoid overfitting.

5. Model III (supervised): f_{im}, f_{label}, & h

Given the promising results on one-shot learning tasks for object recognition, we wanted to assess whether compositional embeddings could be beneficial for multi-label classification in standard supervised learning problems where the testing and training classes are the same (i.e., *not* one-shot). Specifically, we developed a model to answer questions of the form, "Does image x contain an object of class y?". The intuition is that a compositional embedding approach might make the recognition process more accurate by giving it knowledge of *which* object is being queried *before* analyzing the input image for its contents. Model III consists of *three* functions trained jointly: (1) a deep embedding f_{im} for the input image x; (2) a linear layer f_{label} to embed a one-hot vector of the queried label y into a distributed representation; and (3) a query function h that takes the two embeddings as inputs and outputs the probability that the image contains an object with the desired label. This approach enables the combined model to modulate its perception of the objects contained within an image based on the specific task, i.e., the specific label that was queried, which may help it to perform more accurately [20].

5.1. Experiment 4: COCO

To evaluate Model III, we conducted an experiment on the Microsoft COCO dataset [16], which has $|\mathcal{S}| = 80$ classes in both the training and validation sets. During evaluation, half the test labels are positive and the other half are negative.

Architecture: For f_{im}, we modify ResNet-18 (pretrained on ImageNet) so that its last layer has dimension 128. The embedding layer f_{label} maps 80-dimensional 1-hot labels to 32-dimension real-valued embeddings. Then the image embedding and label embedding are concatenated to a 160-dimension vector and fed to the DNN h, consisting of $\text{FC}(160) \rightarrow \text{BN} \rightarrow \text{ReLU} \rightarrow \text{FC}(136) \rightarrow \text{BN} \rightarrow \text{ReLU} \rightarrow \text{FC}(136) \rightarrow \text{Sigmoid}(1)$, where $\text{Sigmoid}(k)$ is a sigmoidal layer with k independent probabilistic outputs. The output of h represents the probability that image x contains an object of class y. See Figure 4 (right). Binary cross-entropy, summed over all classes, is used as the loss function. Because of class imbalance, different weights are used for positive and negative classes according to their numbers in each image.

Baseline: We compare to a baseline consisting of a pretrained ResNet-18 followed by a DNN (to enable a fairer comparison with our Model III). The DNN consists of $\text{FC}(128) \rightarrow \text{BN} \rightarrow \text{ReLU} \rightarrow \text{FC}(128) \rightarrow \text{BN} \rightarrow \text{ReLU} \rightarrow \text{FC}(128) \rightarrow \text{Sigmoid}(80)$. The final layer gives independent probabilistic predictions of the 80 classes. Note that this DNN has almost exactly the same number of parameters as the DNN for Model III. For multi-label image classification, we simply check whether the output for the desired label is close to 1. See Figure 4 (left).

Results: The baseline accuracy using the ResNet attained an accuracy of 64.0% and AUC of 67.7%. In contrast, the compositional embedding approach ($f_{\text{im}} \& f_{\text{label}} \& h$) achieved a substantially higher accuracy of 82.0% and AUC is 90.8%. This accuracy improvement may stem from the task modulation of the visual processing, or from the fact that the compositional method was explicitly designed to answer binary image queries rather than represent the image as a $|\mathcal{S}|$-dimensional vector (as with a standard object recognition CNN).

6. Conclusions

We developed a compositional embedding mechanism whereby the *set* of objects contained in the input data must be both *perceived* and then mapped into a space such that the *set relationships* – union (Model I) and containment (Model II) – between multiple embedded vectors can be inferred. Importantly, the ground-truth rendering process for how examples are rendered from their component classes must implicitly be learned. This new domain of *multi-label one-shot learning* is highly challenging but has interesting applications to multi-object image recognition in computer vision, as well as multi-person speaker recognition and diarization in computer audition. In contrast to prior work [1, 9], our models require only relatively weak one-shot supervision consisting of the label-set relationships among the training examples. Our experiments on OmniGlot, Open Images, and COCO show promising results: the compositional embeddings strongly outperformed baselines based on traditional embeddings. These results provide further evidence that embedding functions can encode rich and complex structure about the *multiple* objects contained in the images they came from. Our results also shed light on how the task structure influences the best design of the functions f, g, and h. Finally, we demonstrated the potential of compositional embeddings for standard supervised tasks of multi-label image recognition (Model III): task-specific perception of images, as enabled by jointly trained embedding functions, can boost perceptual accuracy.

One direction for **future research** – motivated by perceptual expertise research on, for example, how chess experts perceive real vs. random game configurations [4] – is to take better advantage of the class co-occurrence structure in a specific application domain (e.g., which objects co-occur in images).

References

[1] Amit Alfassy, Leonid Karlinsky, Amit Aides, Joseph Shtok, Sivan Harary, Rogerio Feris, Raja Giryes, and Alex M Bronstein. Laso: Label-set operations networks for multi-label few-shot learning. In *Proceedings of the IEEE Conference on Computer Vision and Pattern Recognition*, pages 6548–6557, 2019.

[2] Jacob Andreas. Measuring compositionality in representation learning. *arXiv preprint arXiv:1902.07181*, 2019.

[3] Luca Bertinetto, João F Henriques, Jack Valmadre, Philip Torr, and Andrea Vedaldi. Learning feed-forward one-shot learners. In *Advances in Neural Information Processing Systems*, pages 523–531, 2016.

[4] William G Chase and Herbert A Simon. Perception in chess. *Cognitive psychology*, 4(1):55–81, 1973.

[5] Hanjun Dai, Yichen Wang, Rakshit Trivedi, and Le Song. Deep coevolutionary network: Embedding user and item features for recommendation. *arXiv preprint arXiv:1609.03675*, 2016.

[6] Sounak Dey, Anjan Dutta, Suman K Ghosh, Ernest Valveny, Josep Lladós, and Umapada Pal. Learning cross-modal deep embeddings for multi-object image retrieval using text and sketch. In *2018 24th International Conference on Pattern Recognition (ICPR)*, pages 916–921. IEEE, 2018.

[7] Kaiming He, Xiangyu Zhang, Shaoqing Ren, and Jian Sun. Deep residual learning for image recognition. In *Proceedings of the IEEE conference on computer vision and pattern recognition*, pages 770–778, 2016.

[8] Ting-I Hsieh, Yi-Chen Lo, Hwann-Tzong Chen, and Tyng-Luh Liu. One-shot object detection with co-attention and co-excitation. In *Advances in Neural Information Processing Systems*, pages 2721–2730, 2019.

[9] Dat Huynh and Ehsan Elhamifar. A shared multi-attention framework for multi-label zero-shot learning. In *Proceedings of the IEEE/CVF Conference on Computer Vision and Pattern Recognition*, pages 8776–8786, 2020.

[10] Mandar Joshi, Eunsol Choi, Omer Levy, Daniel S Weld, and Luke Zettlemoyer. pair2vec: Compositional word-pair embeddings for cross-sentence inference. *arXiv preprint arXiv:1810.08854*, 2018.

[11] Gregory Koch, Richard Zemel, and Ruslan Salakhutdinov. Siamese neural networks for one-shot image recognition. In *ICML deep learning workshop*, volume 2, 2015.

[12] Nilesh Kulkarni, Ishan Misra, Shubham Tulsiani, and Abhinav Gupta. 3d-relnet: Joint object and relational network for 3d prediction. In *Proceedings of the IEEE International Conference on Computer Vision*, pages 2212–2221, 2019.

[13] Alina Kuznetsova, Hassan Rom, Neil Alldrin, Jasper Uijlings, Ivan Krasin, Jordi Pont-Tuset, Shahab Kamali, Stefan Popov, Matteo Malloci, Tom Duerig, and Vittorio Ferrari. The open images dataset v4: Unified image classification, object detection, and visual relationship detection at scale. *arXiv:1811.00982*, 2018.

[14] Brenden M Lake and Marco Baroni. Generalization without systematicity: On the compositional skills of sequence-to-sequence recurrent networks. *arXiv preprint arXiv:1711.00350*, 2017.

[15] Brenden M Lake, Ruslan Salakhutdinov, and Joshua B Tenenbaum. Human-level concept learning through probabilistic program induction. *Science*, 350(6266):1332–1338, 2015.

[16] Tsung-Yi Lin, Michael Maire, Serge Belongie, James Hays, Pietro Perona, Deva Ramanan, Piotr Dollár, and C Lawrence Zitnick. Microsoft coco: Common objects in context. In *European conference on computer vision*, pages 740–755. Springer, 2014.

[17] Bingbin Liu, Serena Yeung, Edward Chou, De-An Huang, Li Fei-Fei, and Juan Carlos Niebles. Temporal modular networks for retrieving complex compositional activities in videos. In *Proceedings of the European Conference on Computer Vision (ECCV)*, pages 552–568, 2018.

[18] Tianshu Lyu, Fei Sun, Peng Jiang, Wenwu Ou, and Yan Zhang. Compositional network embedding for link prediction. In *Proceedings of the 13th ACM Conference on Recommender Systems*, pages 388–392, 2019.

[19] Tomas Mikolov, Kai Chen, Greg Corrado, and Jeffrey Dean. Efficient estimation of word representations in vector space. *arXiv preprint arXiv:1301.3781*, 2013.

[20] Michael C Mozer and Adrian Fan. Top-down modulation of neural responses in visual perception: a computational exploration. *Natural Computing*, 7(1):45–55, 2008.

[21] Preslav Nakov, Alan Ritter, Sara Rosenthal, Fabrizio Sebastiani, and Veselin Stoyanov. Semeval-2016 task 4: Sentiment analysis in twitter. In *Proceedings of the 10th international workshop on semantic evaluation (semeval-2016)*, pages 1–18, 2016.

[22] Jeffrey Pennington, Richard Socher, and Christopher Manning. Glove: Global vectors for word representation. In *Proceedings of the 2014 conference on empirical methods in natural language processing (EMNLP)*, pages 1532–1543, 2014.

[23] Jordan B Pollack. Implications of recursive distributed representations. In *Advances in neural information processing systems*, pages 527–536, 1989.

[24] Danilo Jimenez Rezende, Shakir Mohamed, Ivo Danihelka, Karol Gregor, and Daan Wierstra. One-shot generalization in deep generative models. *arXiv preprint arXiv:1603.05106*, 2016.

[25] Rodrigo Santa Cruz, Basura Fernando, Anoop Cherian, and Stephen Gould. Neural algebra of classifiers. In *2018 IEEE Winter Conference on Applications of Computer Vision (WACV)*, pages 729–737. IEEE, 2018.

[26] Florian Schroff, Dmitry Kalenichenko, and James Philbin. Facenet: A unified embedding for face recognition and clustering. In *Proceedings of the IEEE conference on computer vision and pattern recognition*, pages 815–823, 2015.

[27] Tyler Scott, Karl Ridgeway, and Michael C Mozer. Adapted deep embeddings: A synthesis of methods for k-shot inductive transfer learning. In *Advances in Neural Information Processing Systems*, pages 76–85, 2018.

[28] Gregory Sell, David Snyder, Alan McCree, Daniel Garcia-Romero, Jesús Villalba, Matthew Maciejewski, Vimal Manohar, Najim Dehak, Daniel Povey, Shinji Watanabe, et al. Diarization is hard: Some experiences and lessons learned for the jhu team in the inaugural dihard challenge. In *Interspeech*, pages 2808–2812, 2018.

[29] David Snyder, Daniel Garcia-Romero, Gregory Sell, Daniel Povey, and Sanjeev Khudanpur. X-vectors: Robust dnn embeddings for speaker recognition. In *2018 IEEE International Conference on Acoustics, Speech and Signal Processing (ICASSP)*, pages 5329–5333. IEEE, 2018.

[30] Austin Stone, Huayan Wang, Michael Stark, Yi Liu, D Scott Phoenix, and Dileep George. Teaching compositionality to cnns. In *Proceedings of the IEEE Conference on Computer Vision and Pattern Recognition*, pages 5058–5067, 2017.

[31] Tristan Sylvain, Linda Petrini, and Devon Hjelm. Locality and compositionality in zero-shot learning. *arXiv preprint arXiv:1912.12179*, 2019.

[32] Pavel Tokmakov, Yu-Xiong Wang, and Martial Hebert. Learning compositional representations for few-shot recognition. In *Proceedings of the IEEE International Conference on Computer Vision*, pages 6372–6381, 2019.

[33] Kilian Q Weinberger and Lawrence K Saul. Distance metric learning for large margin nearest neighbor classification. *Journal of Machine Learning Research*, 10(Feb):207–244, 2009.

[34] Meng Ye and Yuhong Guo. Deep triplet ranking networks for one-shot recognition. *arXiv preprint arXiv:1804.07275*, 2018.